

DFT modeling, UV-Vis and IR spectroscopic study of acetylacetonate-modified zirconia sol-gel materials

Ivelina Georgieva · Nina Danchova · Stoyan Gutzov ·
Natasha Trendafilova

Received: 3 July 2011 / Accepted: 21 September 2011 / Published online: 12 October 2011
© Springer-Verlag 2011

Abstract Theoretical and spectroscopic studies of a series of monomeric and dimeric complexes formed through the modification of a zirconium butoxide precursor with acetylacetonate and subsequent hydrolysis and/or condensation have been performed by applying DFT/B3LYP/6-31++G(d) and highly accurate RI-ADC(2) methods as well as IR and UV-Vis transmittance and diffuse reflectance spectroscopies. Based on DFT model calculations and simulated and experimental UV-Vis and IR spectra of all the studied structures, the most probable building units of the Zr(IV)–AcAc gel were predicted: the dimeric double hydroxo-bridged complex $Zr_2(AcAc)_2(OH)_4(OH)_{2br}$ **9** and the monooxo-bridged complex $Zr_2(AcAc)_2(OH)_4O_{br} \cdot 2H_2O$ **12**. In both structures, the two AcAc ligands are coordinated to one Zr atom. It was shown that building units **9** and **12** determine the photophysical and vibrational properties of the gel material. The observed UV-Vis and IR spectra of Zr(IV)–AcAc gel were interpreted and a relation between the spectroscopic and structural data was derived. The observed UV-Vis bands at 315 nm and 298/288 nm were

assigned to partial ligand–metal transitions and to intra-/inter-AcAc ligand transitions, respectively.

Keywords Zirconia · Sol-gel · DFT modeling · UV-Vis spectra · IR spectra

Introduction

Sol-gel technology provides a low-temperature method of preparing oxide materials with improved optical or electrical properties using different dopants, such as organic dyes and d- and f-ion complexes. Zirconia is one of the most thoroughly investigated sol-gel systems due to the excellent properties of ZrO_2 material, which have led to its use in porous membranes, matrices in catalysis, and dense dielectric and ferroelectric films in electronics [1–6]. Recently, we synthesized hybrid zirconia sol-gel materials modified with acetylacetonate (AcAc) [7], and demonstrated that modifying agents like AcAc and nitric acid decrease the optical band gap of the sol-gel zirconia from 4.84 eV to about 3 eV. Doping with AcAc leads to yellow-brown materials [7–9]. The well-known color of AcAc-containing zirconia sol-gel materials is caused by Zr(IV)–AcAc complex formation during hydrolysis in the liquid (sol) state, which exhibits strong absorption in the UV region and low-intensity absorption in the visible spectral region [7].

Despite numerous investigations, however, the chemistry and structure of Zr(IV)–AcAc complexes in zirconia gels and during gelation are not well understood. The experimental conditions and precursor used determine the characteristics of the modified zirconia sol-gel. Zr butoxide has been used as a precursor to prepare Zr(IV)–AcAc oxide materials [7]. Its structure has recently been the focus of intense study, and the results of this research seem to be

Electronic supplementary material The online version of this article (doi:10.1007/s00894-011-1257-3) contains supplementary material, which is available to authorized users.

I. Georgieva (✉) · N. Trendafilova
Institute of General and Inorganic Chemistry,
Bulgarian Academy of Sciences,
11 Acad. G. Bonchev Str.,
1113 Sofia, Bulgaria
e-mail: ivelina@svr.igic.bas.bg

N. Danchova · S. Gutzov
Department of Physical Chemistry,
University of Sofia “St. Kliment Ohridski”,
James Bourchier Boulevard 1,
1164 Sofia, Bulgaria

controversial [10–13]. Based on X-ray absorption spectroscopy, EXAFS and XANES, zirconium *n*-butoxide in *n*-butanol was described as consisting of asymmetric tetramers, $Zr_4(BuO)_{16}$ [10]. A similar zirconium tetramer structure with double hydroxo bridging ligands has also been established by X-ray diffraction studies [11]. Bauer et al. proposed a symmetric trimer structure for zirconium *n*-butoxide [12]. Based on NMR data, the species $Zr_3O(BuO)_{10}$ has been suggested to occur in the solid state and in solution [14]. Other authors have argued for monomeric $Zr(BuO)_4$, considering the atomic radius of Zr (1.45 Å), whilst the larger Th atom (radius ~1.65 Å) forms an oligomeric *t*-butoxide complex [15]. The tetrameric complex $Zr_4(OH)_8(H_2O)_{16}Cl_8$ has been identified in both aqueous solution and the solid state [16]. The tetrameric zirconium hydroxyl species could arise from tetrameric Zr butoxide or from concomitant hydrolysis and condensation of monomeric zirconium butoxide, as suggested for the silicon alkoxides. Knowledge of the Zr butoxide structure is important for the reliable prediction and modeling of the AcAc-modified precursor and AcAc-modified zirconia along the reaction steps.

The aim of the work described in this paper was to theoretically and spectroscopically characterize the Zr (IV)–AcAc complexes formed through the modification of the zirconium butoxide precursor with acetylacetone and subsequent hydrolysis and/or condensation, and to compare results obtained with those gained from UV-Vis diffuse reflectance and transmission spectroscopy and IR spectroscopy. DFT modeling and spectral simulations with quantum-chemical methods (DFT and RI-ADC(2)) were applied to determine the complexes that are most likely to be formed during the reaction procedure. Monomeric ($Zr(BuO)_{4-n}(AcAc)_n$, $Zr(OH)_{4-n}(AcAc)_n$, $n=1-4$) and dimeric hydroxo-bridged models were calculated in the gas phase and in solution at the DFT/B3LYP/6-31++G(d) level, and the results were related to the sol species. Dimeric hydroxo- and oxo-bridged Zr(IV)–AcAc models were constructed to represent the repeat units of the ZrO_2 –AcAc gel.

Experimental details

Sample preparation

The samples based on zirconia butoxide as the starting precursor were prepared at room temperature. The syntheses were performed with $Zr(OC_4H_9)_4$ (80% solution in 1-butanol; Aldrich, St. Louis, MO, USA), secondary butanol (99%; Fluka, Buchs, Switzerland), and acetylacetone (99%; Sigma–Aldrich, St. Louis, MO, USA). Acetylacetone was used as a chelating ligand, which resulted in the formation of the

previously described yellow–brown complexes between acetylacetone and zirconium [7]. As a result of the preparation scheme applied (given in Fig. 1), transparent amorphous gels that were colored by the Zr(IV)–AcAc complex were obtained. In this paper, sol and gel species with a molar ratio of reagents n_{Zr}/n_{AcAc} of 0.6 were investigated in detail. The chemical composition (Zr content=42.3% and C content=14.6%) of the sample ($n_{Zr}/n_{AcAc}=0.6$) was determined using an Ultima 2 ICP from Horiba Jobin Yvon (Edison, NJ, USA).

UV-Vis measurements

Room-temperature UV-Vis transmittance and diffuse reflectance spectra of solutions and powdered species were measured on a PerkinElmer (Waltham, MA, USA) Lambda 35 spectrophotometer with a deuterium lamp for the UV region. Optical transmittance spectra of EtOH solutions containing a Zr–AcAc complex ($c_{Zr} \approx 6 \times 10^{-4}$ mol/l, $n_{Zr}/n_{AcAc}=0.6$) were obtained using a 10 mm SUPRASIL (Hellma, Müllheim, Germany) quartz glass cuvette (80% transmittance at 200 nm) and pure ethanol as a reference.

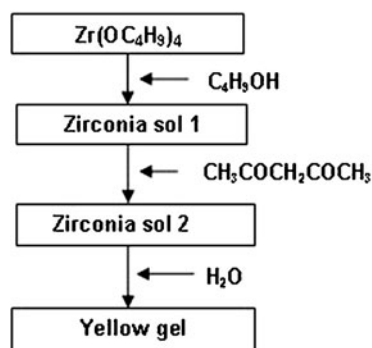
Diffuse reflectance spectra from powdered gels were obtained with a specular reflectance accessory (RSA-PE-20, Labsphere, North Sutton, NH, USA) between 250 and 900 nm. The powders were placed in a black vertical sample holder made in-house from POLIPOM; Fig. 2. The f-f transitions of Ho_2O_3 are used as a reference; both peak positions and intensities were in good agreement with theory between 250 nm and 900 nm [17]. The Kubelka–Munk function $F(R) = \frac{(1-2R)^2}{2R}$ was calculated from the diffuse reflectance $R(\%)$ [18]. The signal/noise ratio in the region 250–300 nm was improved using undoped zirconia sol-gel powders as a white standard.

XRD, IR-spectroscopy, TG/DTA, and analytical characterization

XRD investigations were performed on a Bruker (Billerica, MA, USA) D8 Advance diffractometer with Ni K β filtered radiation and a LynxEye position-sensitive detector (PSD). The results indicated that all of the zirconia samples were X-ray amorphous. The infrared spectra were recorded on a Bruker model IFS 25 Fourier transform interferometer (resolution <2 cm^{-1}) at ambient temperature using KBr discs as matrices.

The thermal stability of the Zr–AcAc sol-gel material was studied using thermogravimetry (TG) and differential thermal analysis (DTA) measurements. DTA/TG was performed on a LABSYS™ EVO apparatus (Setaram, Caluire, France) with Pt/PtRh thermocouples under an air atmosphere. Alumina crucibles were used as vessels at a

Fig. 1 Preparation schemes used for the sol-gel synthesis of zirconia gels (*left*). A typical zirconia gel with $n_{\text{Zr}} / n_{\text{AcAc}} \approx 0.35$ is also shown (*right*)



heating rate of 10 °C/min in the temperature range 25–800 °C. The TG and DTA curves recorded for AcAc-modified zirconia suggest decomposition of the Zr(IV)–AcAc gel via one endothermic weight loss process maximizing at 122.0 °C and three exothermic processes occurring at 261.8, 370.8, and 547.1 °C; see Fig. S1 of the “Electronic supplementary material” (ESM). The endothermic process at 122.0 °C relates to sample dehydration. The exothermic effects (240–660 °C) result from the decomposition/oxidation of the organic matter and the crystallization of tetragonal zirconia nanocrystals during heating [7].

Computational methods

Based on the preparation scheme for the synthesis of AcAc-containing zirconia sol-gel materials, reaction equations were suggested, and the products, monomeric and dimeric Zr–AcAc structures, were modeled (see Table 1). Geometry optimizations of closed shell Zr(IV)–AcAc complexes were performed with DFT and the hybrid B3LYP functional [19,

20] using Gaussian 09 [21]. The 6-31++G(d) basis set was used for carbon, oxygen (11s5p1d)/[4s3p1d], and hydrogen ((5s)/[3s]) atoms. The effective quasi-relativistic core potential ECP28MWB and the corresponding basis set were used for the Zr atom (8s7p6d/[6s5p3d] [22]. The ECP28MWB treats [Ar]3d¹⁰ as a core, whereas 4s²4p⁶4d⁰5s⁰ shells are taken into account explicitly. Full geometry optimizations were carried out without symmetry constraints. The structural minima were qualified by the absence of negative eigenvalues in the diagonalized Hessian matrix, giving an imaginary normal vibrational mode. The IR spectra of the model complexes were simulated using the DFT/B3LYP/6-31++G(d) method, and approximate assignments of the calculated frequencies to the molecular vibrational modes were performed based on the atom movements in Cartesian coordinates calculated with the Gaussian program. The calculated atom movements were further used as an input for the ChemCraft program, which animates them and makes it possible to visually inspect each molecular mode [23]. To explore the experimental UV-Vis data of Zr(IV)–AcAc complexes

Fig. 2 Sample holder used for diffuse reflectance measurements of powder samples

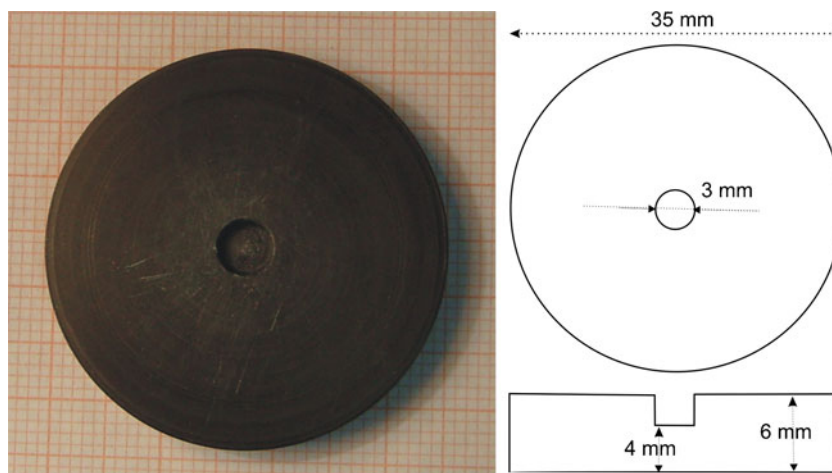


Table 1 Reaction equations and structures of the Zr–AcAc products obtained by following the preparation scheme (Fig. 1) for sol-gel synthesis. The geometries were optimized at the DFT/B3LYP/6-31++G(d) level (ECPMWB28 potential for Zr)

Reaction	Structure	No
<p>1.1. exchange reaction</p> $\text{Zr}(\text{BuO})_4 + \text{AcAc} \rightarrow \text{Zr}(\text{AcAc})(\text{BuO})_3 + \text{BuOH} \quad (1)$		1
<p>1.2. exchange reaction</p> $\text{Zr}(\text{BuO})_4 + 2\text{AcAc} \rightarrow \text{Zr}(\text{AcAc})_2(\text{BuO})_2 + 2\text{BuOH} \quad (2)$		2
<p>1.3. exchange reaction</p> $\text{Zr}_4(\text{BuO})_{16} + 2\text{AcAc} \rightarrow \text{Zr}_4(\text{AcAc})_2(\text{BuO})_{14} + 2\text{BuOH} \quad (3)$	<p style="text-align: center;">3a 3b 3c</p> <p style="text-align: center;">R = Bu [10]</p>	3 ^a
<p>2.1. hydrolysis reaction</p> $\text{Zr}(\text{AcAc})(\text{BuO})_3 + 5\text{H}_2\text{O} \rightarrow \text{Zr}(\text{AcAc})(\text{OH})_3 \cdot 2\text{H}_2\text{O} + 3\text{BuOH} \quad (4)$		4
<p>2.2. hydrolysis reaction</p> $\text{Zr}(\text{AcAc})_2(\text{BuO})_2 + 4\text{H}_2\text{O} \rightarrow \text{Zr}(\text{AcAc})_2(\text{OH})_2 \cdot 2\text{H}_2\text{O} + 2\text{BuOH} \quad (5)$		5

measured in polar solution, the absorption spectra of the optimized geometries in butanol were calculated in the same solution at the TDDFT/B3LYP/6-31++G(d) level. A nonequilibrium implementation of the polarizable continuum model (PCM) using the integral equation formalism variant (IEFPCM) was applied to simulate the solvent effects [24–26]. To overcome the failure of TDDFT to calculate the correct charge-transfer transition, the vertical excitation energies of Zr(IV)–AcAc complexes were calculated with highly accurate resolution-of-the-identity algebraic diagrammatic construction through a second-order (RI-ADC(2)) method [27, 28] using the def2-SVP basis for all atoms

and the effective core potential ECP28MWB for the Zr atom [29, 30]. When used in combination with the resolution of the identity (RI) procedure [31], ADC(2) is a computationally very efficient approach that incorporates dynamical electron correlation effects. The recent introduction of linear response theory (LRT) in combination with analytic gradients [32] provides the capacity to treat excited states. The RI-ADC(2) calculations were performed with the Turbomole6.1 software package [33]. The character of the molecular orbitals that contribute to the most intense transitions was analyzed by means of Mulliken and natural population analyses (NPA) [34].

Table 1 (continued)

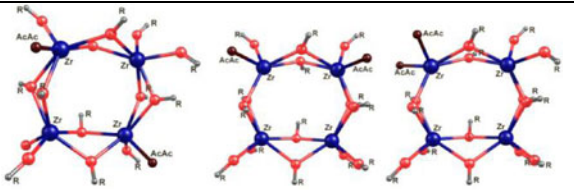
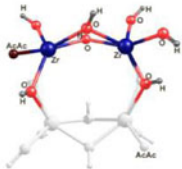
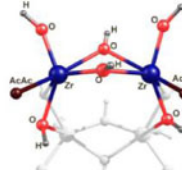
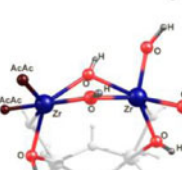
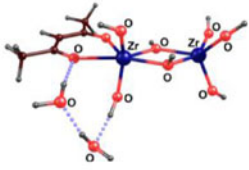
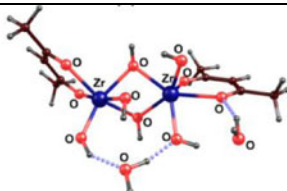
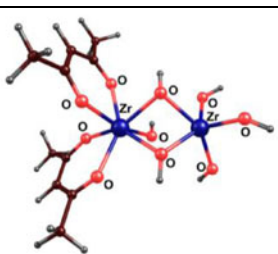
Reaction	Structure	No
<p>2.3. hydrolysis reaction</p> $\text{Zr}_4(\text{AcAc})_2(\text{BuO})_{14} + 14\text{H}_2\text{O} \rightarrow \text{Zr}_4(\text{AcAc})_2(\text{OH})_{14} + 14\text{BuOH} \quad (6)$ <p>Cluster approach to 6</p> $\text{Zr}_2(\text{AcAc})(\text{OH})_5(\text{OH})_{2\text{br}}$ $\text{Zr}_2(\text{AcAc})_2(\text{OH})_4(\text{OH})_{2\text{br}}$ $\text{Zr}_2(\text{AcAc})_2(\text{OH})_4(\text{OH})_{2\text{br}}$	 ${}^a\text{R}=\text{OH}$   	<p>6^a</p> <p>7^{a,b}</p> <p>8^{a,b}</p> <p>9^{a,b}</p>
<p>3.1.1. condensation reaction of hydrolyzed monomeric Zr(IV)-AcAc complexes</p> $\text{Zr}(\text{AcAc})(\text{OH})_3 + \text{Zr}(\text{OH})_4 + 2\text{H}_2\text{O} \rightarrow \text{Zr}_2(\text{AcAc})(\text{OH})_5(\text{OH})_{2\text{br}} + 2\text{H}_2\text{O} \quad (7)$		<p>7^b</p>
<p>3.1.2. condensation reaction of hydrolyzed monomeric Zr(IV)-AcAc complexes</p> $\text{Zr}(\text{AcAc})(\text{OH})_3 + \text{Zr}(\text{AcAc})(\text{OH})_3 + 2\text{H}_2\text{O} \rightarrow \text{Zr}_2(\text{AcAc})_2(\text{OH})_4(\text{OH})_{2\text{br}} + 2\text{H}_2\text{O} \quad (8)$		<p>8^b</p>
<p>3.2. condensation reaction of hydrolyzed monomeric Zr(IV)-AcAc complexes</p> $\text{Zr}(\text{AcAc})_2(\text{OH})_2 + \text{Zr}(\text{OH})_4 \rightarrow \text{Zr}_2(\text{AcAc})_2(\text{OH})_4(\text{OH})_{2\text{br}} \quad (9)$		<p>9</p>

Table 1 (continued)

Reaction	Structure	No
4.1.1 dehydroxylation reaction (formation of monooxo-bridges -O-) $\text{Zr}_2(\text{AcAc})_2(\text{OH})_4(\text{OH})_{2\text{br}} \cdot 4\text{H}_2\text{O} \rightarrow$ $\text{Zr}_2(\text{AcAc})_2(\text{OH})_4\text{O}_{\text{br}} \cdot 4\text{H}_2\text{O} + \text{H}_2\text{O}$ (10)		10
4.1.2 dehydroxylation reaction (formation of double oxo-bridges -O-) $\text{Zr}_2(\text{AcAc})_2(\text{OH})_4(\text{OH})_{2\text{br}} \cdot 4\text{H}_2\text{O} \rightarrow$ $\text{Zr}_2(\text{AcAc})_2(\text{OH})_2\text{O}_{2\text{br}} \cdot 4\text{H}_2\text{O} + 2\text{H}_2\text{O}$ (11)		11
4.2.1. dehydroxylation reaction (formation of monooxo-bridges -O-) $\text{Zr}_2(\text{AcAc})_2(\text{OH})_4(\text{OH})_{2\text{br}} \cdot 2\text{H}_2\text{O} \rightarrow$ $\text{Zr}_2(\text{AcAc})_2(\text{OH})_4\text{O}_{\text{br}} \cdot 2\text{H}_2\text{O} + \text{H}_2\text{O}$ (12)		12
4.2.2. dehydroxylation reaction (formation of double oxo-bridges -O-) $\text{Zr}_2(\text{AcAc})_2(\text{OH})_4(\text{OH})_{2\text{br}} \cdot \text{H}_2\text{O} \rightarrow$ $\text{Zr}_2(\text{AcAc})_2(\text{OH})_2\text{O}_{2\text{br}} \cdot \text{H}_2\text{O} + 2\text{H}_2\text{O}$ (13)		13

^a Scheme^b For simplicity, the number denotes the main molecule structure (without the outside coordination sphere of hydrogen-bonded water molecules)

Results and discussion

Monomeric Zr(IV)–AcAc complexes and dimeric hydroxyl-bridged Zr(IV)–AcAc complexes formed in solution The AcAc-modified Zr(IV) butoxide precursor and AcAc-modified zirconia species obtained in solution are now discussed in accordance with the reaction scheme shown in Fig. 1 and supported by the known chemistry of Zr butoxide and Zr–AcAc complex formation [1–16, 35, 36]. Initially, zirconia sol 1 is obtained from Zr butoxide in *n*-butanol solution, and, based on previous studies, the formation of monomeric [16] or tetrameric $\text{Zr}_4(\text{BuO})_{16}$ [10] complexes would be expected here. According to EXAFS and SAXS studies, four Zr atoms form a ring, and each Zr atom is linked to other two Zr atoms by double oxygen bridges (BuO). Two single and four bridging BuO groups are connected to the six-coordinated Zr(IV) center, as shown in Fig. 3.

The second stage involves the reaction of zirconium butoxide (monomeric $\text{Zr}(\text{BuO})_4$ or tetrameric $\text{Zr}_4(\text{BuO})_{16}$) with AcAc in butanol solution and the formation of mixed-ligand Zr–BuO/AcAc complexes (zirconia sol 2). Considering a monomeric $\text{Zr}(\text{BuO})_4$ precursor in the complexation reaction with the AcAc ligand, the formation of the complexes $\text{Zr}(\text{AcAc})(\text{BuO})_3$ (1) and $\text{Zr}(\text{AcAc})_2(\text{BuO})_2$ (2) is anticipated, corresponding to reactions (1) and (2), respectively, in Table 1 [15]. The $\text{Zr}(\text{AcAc})_3(\text{BuO})$ complex is unstable in solution in the absence of hydrolysis, so it is not considered further here [37]. The complete exchange of all BuO ligands and formation of the most stable complex, $\text{Zr}(\text{AcAc})_4$, is unlikely because of the low AcAc ligand concentrations used in our experiment. In the case of a tetrameric $\text{Zr}_4(\text{BuO})_{16}$ precursor in butanol [10] and the molar ratio $n_{\text{AcAc}}/n_{\text{Zr}}=0.6$, we expect that all of the $\text{Zr}_4(\text{BuO})_{16}$ reacts with AcAc to produce the compound

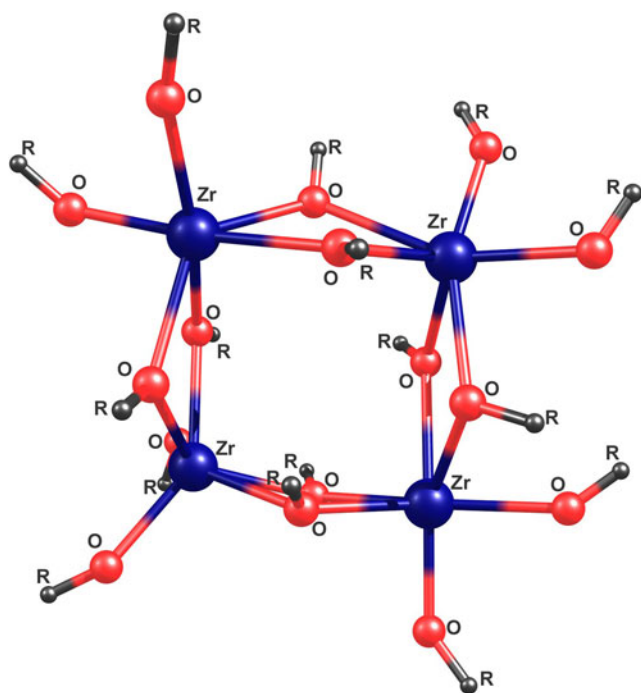


Fig. 3 The tetramer Zr(IV) structure, as experimentally demonstrated in solution [10] (R = Bu, H)

$Zr_4(\text{AcAc})_2(\text{BuO})_{14}$ (**3**); see reaction (3) in Table 1. In the modified complex, the two BuO^- groups that are linked to non-neighboring Zr atoms, to neighboring Zr atoms, or to one Zr atom could be replaced by two chelating AcAc ligands. Hence, the formation of three $Zr_4(\text{AcAc})_2(\text{BuO})_{14}$ species (**3a**, **3b**, **3c**) is suggested; see Table 1. Based on preparation steps 1 and 2 (Fig. 1) and the chemistry of Zr butoxide, three compounds of zirconia sol 2 (**1**, **2**, and **3**; Table 1) are thought to be produced in butanol solution. These complexes are further discussed as potential AcAc-modified Zr butoxide precursors in the sol-gel process, including hydrolysis and condensation reactions.

An experimental study on the hydrolytic stability of organic ligands in metal alkoxide complexes has shown that the AcAc (95–100%) has high hydrolytic stability due to its strong chelate bonding to the metal, meaning that only hydrolysis of the alkoxo groups proceeds [38]. In the reaction scheme used in this study, the amount of water is dominant ($n_{\text{BuOH}}:n_{\text{H}_2\text{O}} = 1:4$), and we accept that the hydrolysis reaction goes to completion (all BuO groups are replaced by OH groups). As a result of the hydrolysis processes (4–6) in Table 1, the complexes $Zr(\text{AcAc})(\text{OH})_3$ (**4**), $Zr(\text{AcAc})_2(\text{OH})_2$ (**5**) or $Zr_4(\text{OH})_{14}(\text{AcAc})_2$ (**6**) should be obtained. Since the computation of the large tetramer structure is very time-consuming, we divided cluster **6** into three dimer fragments with double hydroxo (OH) bridges linking both Zr atoms: $Zr_2(\text{AcAc})(\text{OH})_5(\text{OH})_{2\text{br}}$ (**7**) and two $Zr_2(\text{AcAc})_2(\text{OH})_4(\text{OH})_{2\text{br}}$ complexes (**8**, **9**), where the

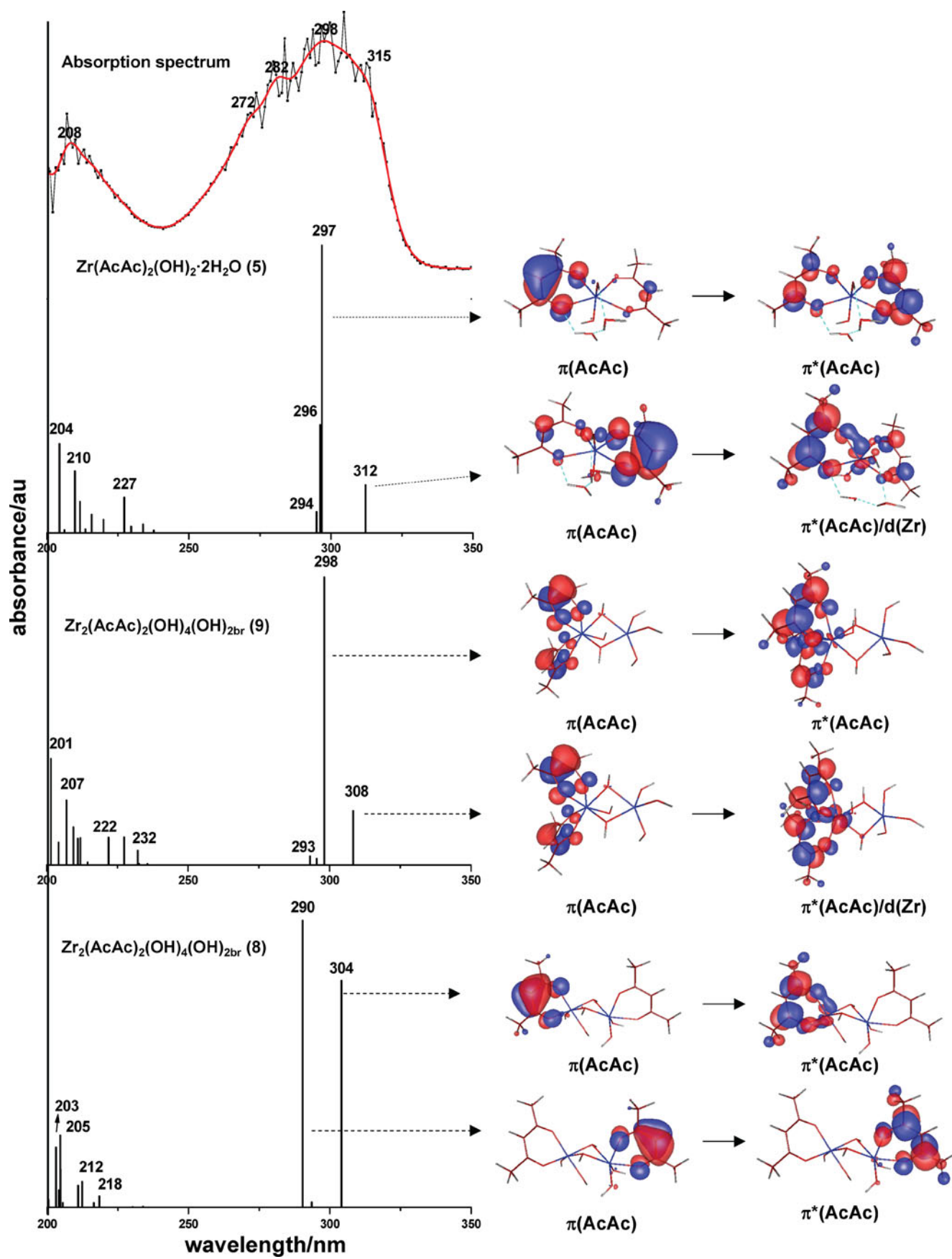
AcAc ligands are connected to different Zr atoms and to one Zr atom, respectively; see Table 1.

The hydrolysis is usually accompanied by a dimerization or condensation reaction, which results in the formation of larger Zr-containing molecules that form chains or rings. Therefore, dimerization between the hydrolyzed monomeric Zr(IV)–AcAc complexes $Zr(\text{AcAc})(\text{OH})_3$ or $Zr(\text{AcAc})_2(\text{OH})_2$ and $Zr(\text{OH})_4$ ($n_{\text{AcAc}}:n_{\text{Zr}}=0.6$) in solution should be expected, and the condensation reactions (7), (8), and (9) were assumed to occur, Table 1. The dimeric double hydroxo-bridged Zr(IV)–AcAc products **7**, **8**, and **9** of the reactions above appear to form the same kind of clusters already included in our discussion of the hydrolyzed tetrameric Zr(IV)–AcAc complex above (see cluster approach to **6** in Table 1).

The chemical analysis performed in this study, as well as our recent results [7], suggest the presence of both physically and chemically bonded water in the sol-gel glasses. The results thus obtained are further used to simulate the hygroscopic moisture. In the structural models studied below, water molecules that are hydrogen bonded to the ligand oxygen atoms (AcAc and OH) are included.

DFT modeling and UV-Vis spectra simulations [TDDFT and ADC(2)] of monomeric and dimeric hydroxo-bridged Zr(IV)–AcAc complexes in solution To obtain data on the molecular geometries of Zr(IV)–AcAc complexes formed in butanol/aqueous solution, two groups of model complex structures were considered in the gas phase at the DFT level: monomeric (**4**, **5**) and dimeric double hydroxo-bridged (**7**, **8**, **9**); see Table 1. Dimeric Zr(IV)–AcAc complexes with double hydroxo bridging have been reported in the literature, and data on their structures are available [39]. The vertical excitation energies were calculated in the gas phase and in butanol solution at the corresponding optimized geometries of the model Zr(IV)–AcAc complexes by applying the TDDFT/B3LYP/6-31++G (d) method. Comparison of the calculated vertical excitation energies at the TDDFT level in the gas phase and in solution showed that the solvent effect is small (~ 5 nm). This finding led us to perform the absorption spectra calculations in the gas phase using the highly accurate RI-ADC(2) method. The simulated UV-Vis spectra of the model Zr(IV)–AcAc complexes **4**, **5**, **7–9** (at the RI-ADC(2) level) were compared to the experimental absorption spectrum in solution to suggest the most probable complex formed in solution. The experimental absorption spectrum of the Zr(IV)–AcAc complex and the calculated ones of **5**, **9**, **8** are shown in Fig. 4, while those of **4** and **7** are given in Fig. 5.

The experimental UV-Vis spectrum of a sample with the molar ratio $n_{\text{AcAc}}/n_{\text{Zr}} = 0.6$ in solution shows an intense band at 298 nm, a medium band at 208 nm, and a shoulder at 315 nm. All of the calculated UV-Vis spectra of the model Zr



◀ **Fig. 4** Experimental UV-Vis spectrum of Zr–AcAc sol ($n_{\text{AcAc}}/n_{\text{Zr}}=0.6$) compared to simulated ones of $\text{Zr}(\text{AcAc})_2(\text{OH})_2 \cdot 2\text{H}_2\text{O}$ (5), $\text{Zr}_2(\text{AcAc})_2(\text{OH})_4(\text{OH})_{2\text{br}}$ (9) and $\text{Zr}_2(\text{AcAc})_2(\text{OH})_4(\text{OH})_{2\text{br}} \cdot 2\text{H}_2\text{O}$ (8). Vertical excitation energies and oscillator strengths were calculated with the RI-ADC(2) method

(IV)–AcAc complexes studied (Fig. 4 and Fig. 5) exhibit a strong band in the region 290–298 nm, which corresponds well to the most intense experimental absorption band at 298 nm. Based on the molecular orbitals, this band was assigned mainly to the intra/interligand $\pi(\text{AcAc}) \rightarrow \pi^*(\text{AcAc})$ transition. The experimental UV-Vis spectrum displays a clearly distinguish-

able shoulder at ~315 nm; see Fig. 4. Such a shoulder was calculated for the model structures 5 and 9, shown in Fig. 4. In the calculated spectra of the model structures 4 and 7, however, the shoulder at ~315 nm is missing (Fig. 5), and only one intense band at ~294 nm is predicted. Obviously, the simulated spectra of the model structures 4 and 7 with one AcAc ligand attached to a Zr atom do not agree with the experimental one, so these two models (considered to be less probable) are not discussed further here.

The best agreement with the experimental spectrum was achieved for model structures 5 and 9 (Fig. 4), where the

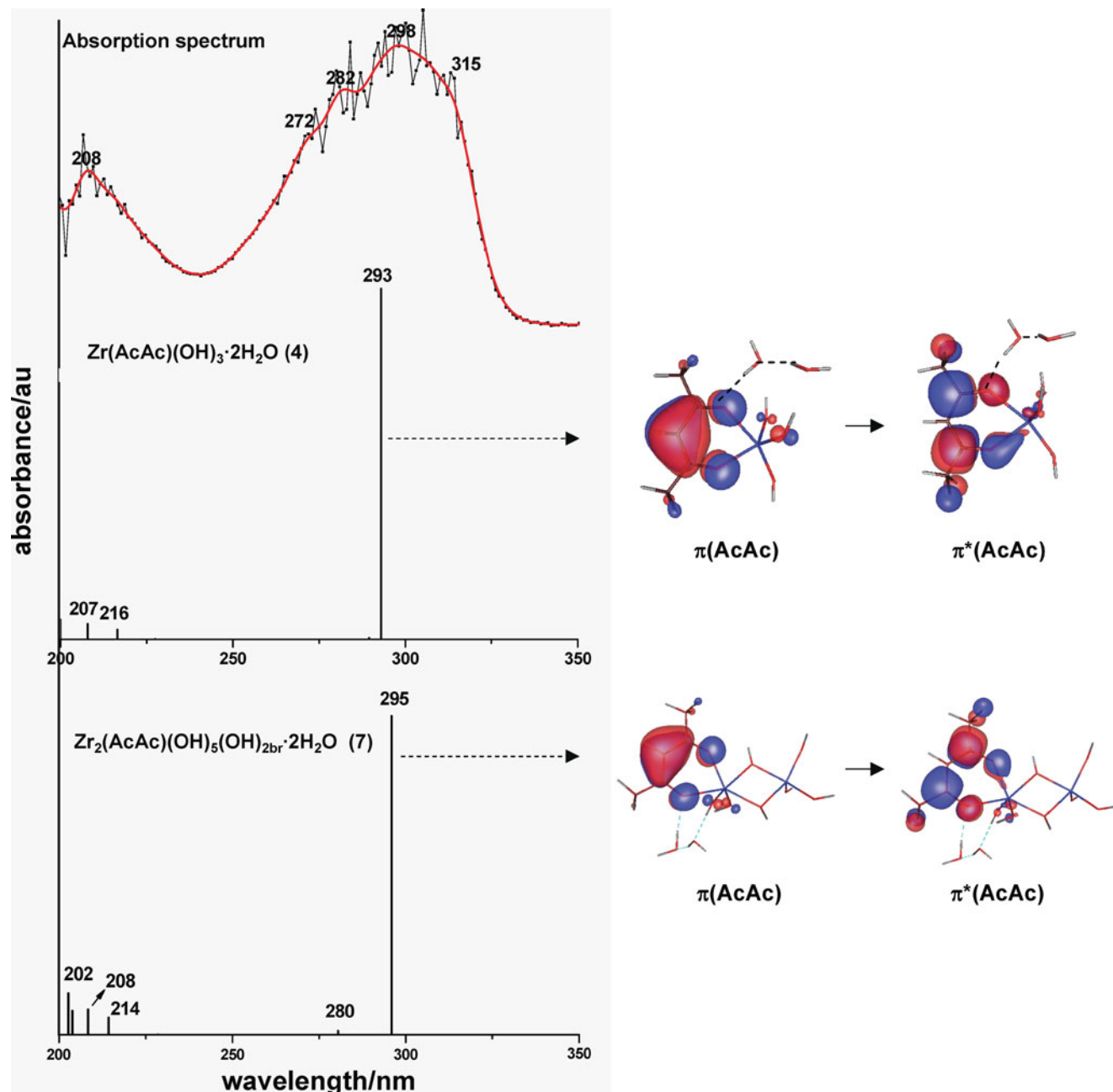


Fig. 5 Experimental UV-Vis spectrum of Zr–AcAc sol ($n_{\text{AcAc}}/n_{\text{Zr}}=0.6$) compared to simulated ones of $\text{Zr}(\text{AcAc})(\text{OH})_3 \cdot 2\text{H}_2\text{O}$ (4) and $\text{Zr}_2(\text{AcAc})(\text{OH})_5(\text{OH})_{2\text{br}} \cdot 2\text{H}_2\text{O}$ (7). Vertical excitation energies and oscillator strengths were calculated with the RI-ADC(2) method

two AcAc ligands are bound to one Zr atom. The monomeric complex **5** and the dimeric complex **9** showed similar absorption properties, despite their different structures. Hence, we can conclude that the monomeric Zr(IV)–AcAc unit is the main source of the photophysical properties of the larger Zr chains or rings in the zirconia sol-gel material. The characteristic bands at 312/308, 297/298, and 204/207 nm calculated for **5** and **9** are consistent with the observed bands at 315, 298, and 208 nm for the Zr(IV)–AcAc sol; see Fig. 4. The bands are due mainly to $\pi(\text{AcAc}) \rightarrow \pi^*(\text{AcAc})/d(\text{Zr})$, $\pi(\text{AcAc}) \rightarrow \pi^*(\text{AcAc})$ and $\pi(\text{AcAc}/\text{OH}) \rightarrow \pi^*(\text{AcAc})/d(\text{Zr})$ transitions, respectively. Thus, the bands at 312 and 208 nm have partial L→M charge-transfer character. In summary, the simulated absorption spectra, when compared to the experimental one, predicted that the monomeric complex **5** and the dimeric double hydroxo-bridged complex **9** are the complexes that are most likely to form in solution. It should be mentioned, however, that the monomeric structure **5** probably occurs in solution, but it needs significant reorganization to become a suitable unit for forming and growing a chain in the gel material. Therefore, structure **5** will not be discussed further here.

The calculated UV-Vis spectrum of the dimeric double hydroxo-bridged structure **8** with two AcAc bound to neighboring Zr atoms showed two intense bands at 304 nm and 290 nm, which are due to intraligand $\pi(\text{AcAc}) \rightarrow \pi^*(\text{AcAc})$ transitions; see Fig. 4. These bands arise from the presence of two **4** units, which produce one intense UV-Vis band at 293 nm. The calculated bands at 304 nm, 290 nm, and 205 nm may be related to the observed bands at 315 nm, 298 nm, and 208 nm, so structure **8** could also be considered a potential repeat unit in gel formation.

DFT modeling and UV-Vis spectra simulations [RI-ADC (2)] of dimeric monooxo-bridged and double oxo-bridged Zr(IV)–AcAc units in solid gels The sol-gel process involves condensation reactions and dehydroxylation (the formation of oxo bridges –O–), and thus the formation of polymeric species with mono- (or double) hydroxo (–OH) or oxo (–O–) bridges is expected [40–43]. These oligomers consist of repeat units that determine the main photophysical and vibrational properties of the zirconia gel material. To study these properties, we applied a comprehensive cluster approach. We expect the hydroxo-bridged Zr–AcAc structures **8** and **9**, formed in solution (sol), to participate as building units in the Zr–AcAc gel (during the process of gelation). In addition, we performed DFT modeling of the dimeric monooxo-bridged $\text{Zr}_2(\text{AcAc})_2(\text{O}-\text{H})_4\text{O}_{\text{br}} \cdot 4\text{H}_2\text{O}$ (**10**) and $(\text{AcAc})_2(\text{OH})_4\text{O}_{\text{br}} \cdot 2\text{H}_2\text{O}$ (**12**) and the double oxo-bridged $\text{Zr}_2(\text{AcAc})_2(\text{OH})_2\text{O}_{2\text{br}} \cdot 4\text{H}_2\text{O}$ (**11**) and $\text{Zr}_2(\text{AcAc})_2(\text{OH})_2\text{O}_{2\text{br}} \cdot \text{H}_2\text{O}$ (**13**) structures obtained by

dehydroxylation reactions (10–13); see Table 1. The calculated vertical excitation energies of dimeric structures **10–13** were compared to the diffuse reflectance spectrum of the Zr(IV)–AcAc gel material; see Fig. 6. The visualized molecular orbitals in Fig. 6 reveal the nature of the corresponding energy transitions. The experimental reflectance spectrum reveals an absorption band at ~316 nm and an intense band at ~288 nm, and this is similar to those seen for the Zr(IV)–AcAc sol in solution (two bands at 315 and 298 nm).

As seen from Fig. 6, the best agreement with the experimental spectrum was achieved for the dimeric monooxo bridged Zr(IV)–AcAc structure **12**: a band at 295 nm due to the $\pi(\text{AcAc}) \rightarrow \pi^*(\text{AcAc})$ transition, and a band at 313 nm due to the $\pi(\text{AcAc}) \rightarrow \pi^*(\text{AcAc})/d(\text{Zr})$ transition; i.e., it has partial L-M charge transfer character. In contrast to structure **12**, the simulated spectra of the dimeric oxo-bridged structures **10**, **11**, and **13** show two transition bands that are very close in energy: at 294 and 298 nm, at 299 and 297 nm, and at 308 and 306 nm, respectively. In all of them, the absorption band at 316 nm is missing. As they are not completely in accord with the experimental results, structures **10**, **11**, and **13** are considered unlikely.

In summary, based on the calculated absorption and experimental reflectance spectra, the hydroxo-bridged structure **9** and the oxo-bridged structure **12** (two AcAc ligands are connected to one Zr atom) are considered to be the most likely building blocks for the Zr(IV)–AcAc gel material. Structure **8** appears less probable, but is also considered to be a possible unit in the solid state. Further, confirmation of the suggested structural units can be found in the vibrational study of the Zr(IV)–AcAc gel material.

IR spectra simulations and vibrational analysis

To verify the dimeric Zr(IV)–AcAc structural units of the zirconia sol-gel material, we performed detailed vibrational analysis based on a comparison of the calculated IR frequencies of the model dimeric structures **8**, **9**, and **12** (suggested above) with the experimental IR spectrum of Zr(IV)–AcAc gel material; see Fig. 7. The IR spectra of the other dimeric structures (monooxo-bridged **10** and double oxo-bridged **11** and **13**) are given for comparison in Fig. S2 of the ESM.

According to IR calculations of the microsolvated dimeric Zr(IV)–AcAc complexes, the observed broad intense band at 3417 cm^{-1} is due to $\nu(\text{OH})$ vibrations. The position of this band confirms the suggestion regarding H-bonded solvent molecules (H_2O) and H-bonded OH groups attached to the Zr atom. Free water molecules and free OH ligands should produce low-intensity $\nu(\text{OH})$ bands at higher frequencies $\sim 3700 \text{ cm}^{-1}$ than those observed

Fig. 6 The diffuse reflectance spectrum of Zr(IV)–AcAc gel compared to the calculated absorption spectra of monooxo-bridged and double oxo-bridged model Zr complexes **10–13**. Vertical excitation energies and oscillator strengths were calculated with the RI-ADC(2) method

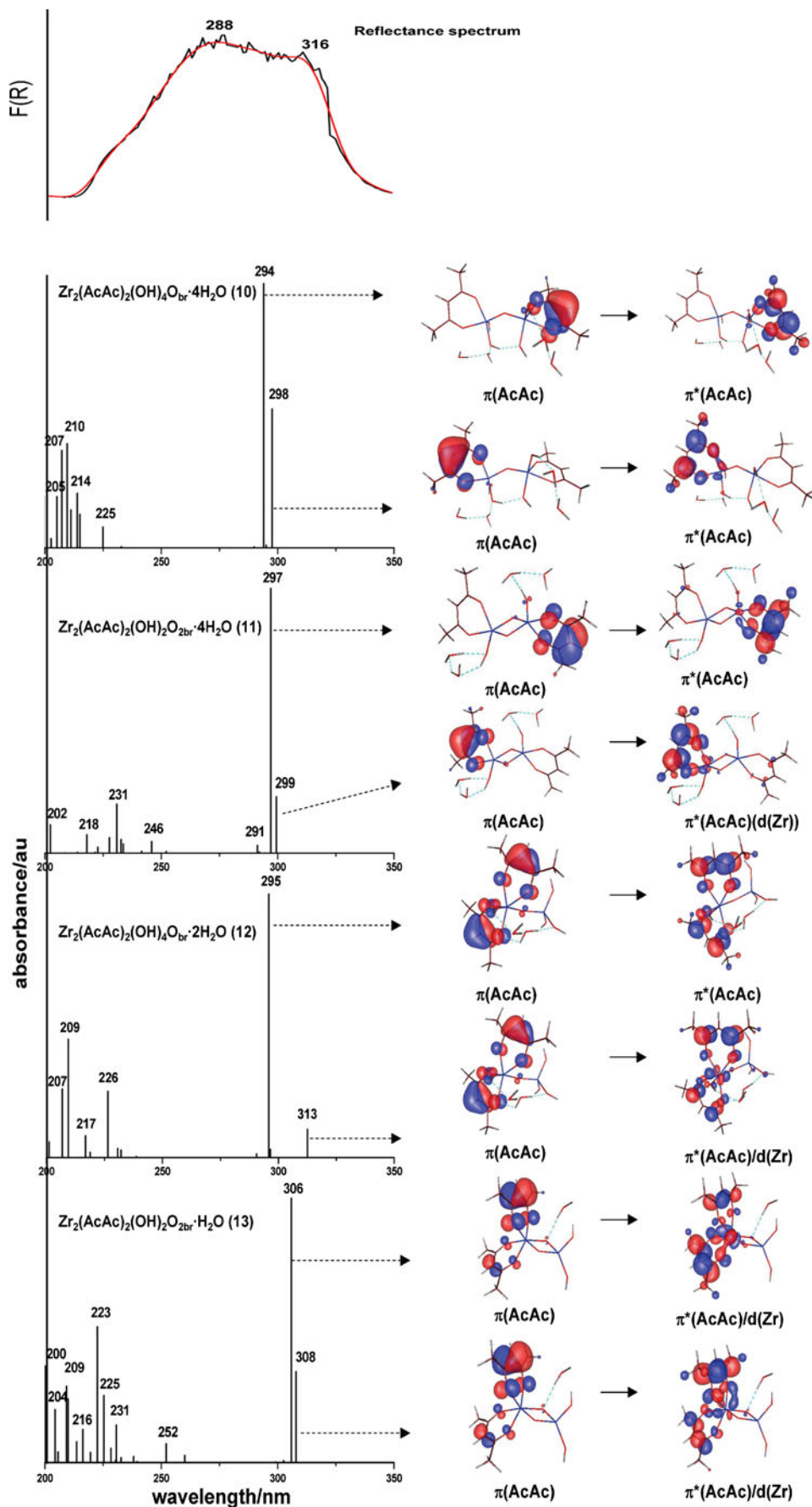
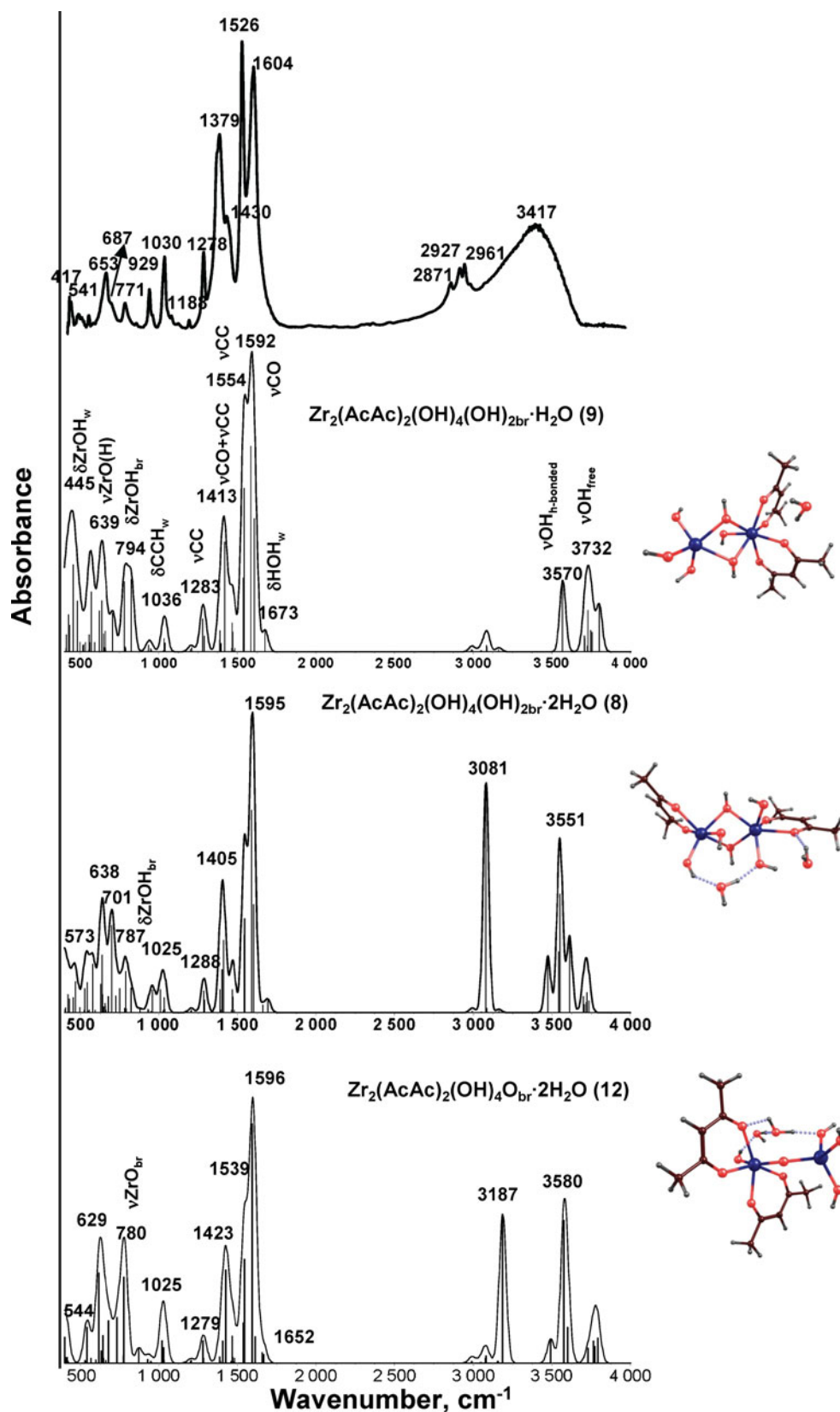


Fig. 7 Experimental IR spectrum of the Zr–AcAc gel and B3LYP/6-31++G(d) IR spectra (scale factor: 0.98) of the dimeric complexes $Zr_2(\text{AcAc})_2(\text{OH})_4(\text{OH})_{2\text{br}}\cdot\text{H}_2\text{O}$ (**9**), $Zr_2(\text{AcAc})_2(\text{OH})_4(\text{OH})_{2\text{br}}\cdot 2\text{H}_2\text{O}$ (**8**) and $Zr_2(\text{AcAc})_2(\text{OH})_4\text{O}_{\text{br}}\cdot 2\text{H}_2\text{O}$ (**12**)



$\sim 3417\text{ cm}^{-1}$. The broadening of the band at 1604 cm^{-1} suggests an overlapped vibration due to the bending $\delta(\text{HOH})$ mode of the water molecules. According to the

calculations, the $\rho(\text{HOH})$ and $\delta(\text{OH}\cdots\text{O})$ vibrations should appear at $\sim 650\text{ cm}^{-1}$ and $\sim 850\text{ cm}^{-1}$. However, these bands are not distinct, since the Zr–OH group vibrations are found

in the same region. Thus, the broad intense band at 3417 cm^{-1} and the low-intensity shoulder at $\sim 1680\text{--}1640\text{ cm}^{-1}$ are indicative of hydrogen-bonded water molecules in the Zr(IV)–AcAc system, in agreement with TG/DTA measurements.

The calculated IR spectra of the dimeric Zr(IV)–AcAc complexes **8**, **9**, and **12** confirmed the bidentate binding of the AcAc ligand to the Zr atom. The bands observed at 1604 and 1379 cm^{-1} , assigned to $\nu(\text{CO})$ vibrations of AcAc, are indicative of the bidentate binding of AcAc; see Fig. 7. The bands are shifted to lower frequencies ($\sim 150\text{ cm}^{-1}$) than free acetylacetone [44]. The bands at 1526 and 1278 cm^{-1} are attributed to $\nu(\text{CC})$ vibrations, whereas the bands at 1188 , 1030 , and 929 cm^{-1} are due to bending $\delta(\text{CCH})$ mixed with stretching $\nu(\text{CC})$ vibrations. According to the calculations, $\nu(\text{Zr–O}_{\text{AcAc}})$ vibrations should appear at $415\text{--}430\text{ cm}^{-1}$ with medium band intensity.

The butoxide group should produce an intense band in the $1050\text{--}1150\text{ cm}^{-1}$ region [45]. Such an intense band at 1050 cm^{-1} was observed for $\text{Zr}(\text{OBU})_{4-n}(\text{AcAc})_n$ complexes in [37, 42]. In line with data in the literature, our IR spectra calculations of complexes **1** and **2** (Table 1) predicted a very strong $\nu(\text{CO})_{\text{BuO}}$ band at $\sim 1110\text{ cm}^{-1}$. However, the experimental IR spectrum of the zirconia gel material modified with AcAc does not show such an intense band, indicating the absence of a butoxide group in the material. The calculated and experimental IR spectra confirmed our suggestion that during the sol-gel process in solution, all of the BuO groups in the Zr complex are replaced with OH groups.

A detailed analysis of the IR spectra was performed to search for a vibrational criterion that can distinguish the bridging type, considering double hydroxo-bridging structures **9** and **8** and monooxo-bridging structures **12** (Fig. 7) and **10** (see Fig. S2 of the ESM).

Our IR calculations for the models **8** and **9** showed that the medium bands in the region $822\text{--}770\text{ cm}^{-1}$ are due to characteristic bending $\delta(\text{Zr–O–H})_{\text{br}}$ vibrations; see Fig. 7. Such a band should be indicative of a hydroxo bridge in the Zr(IV)–AcAc material, since there is no vibration of the AcAc ligand in the region $930\text{--}700\text{ cm}^{-1}$. This vibration was found for the hydroxo-bridged metal complexes in the range ca. $1000\text{--}677\text{ cm}^{-1}$ [39, 46]. The $\text{Zr–O}(\text{H})_{\text{br}}$ group exhibits out-of-plane bending and stretching $\nu(\text{Zr–O})$ vibrations below 600 cm^{-1} , which are mixed with Zr–OH vibrations and overlap, so they are not informative.

At the same time, the calculated IR spectrum of structure **12** showed an intense band at 780 cm^{-1} due to the $\nu(\text{Zr–O}_{\text{br}})$ stretching vibration; see Fig. 7. The same intense $\nu(\text{Zr–O}_{\text{br}})$ band at 775 cm^{-1} was detected for the monooxo-bridged structure **10**. Such a strong band at 766 cm^{-1} attributed to vibrations of the mono Ti–O–Ti bridge was

detected by a variable temperature IR study of Ti species containing multinuclear oxo clusters in the gas phase [47].

In summary, the calculated IR spectra and assignments of the vibrational frequencies confirmed the presence of hydrogen-bonded water molecules, the absence of any butoxide group, and the bidentate binding of the AcAc ligands to the Zr atom in the Zr(IV)–AcAc material. However, the calculated IR spectra cannot help to distinguish between structures with double hydroxo bridging and those with monooxo bridging. Since a medium band at 771 cm^{-1} is observed in the IR spectrum of Zr(IV)–AcAc gel, both double hydroxo- and monooxo-bridged structures are possible. The calculated spectra of **9** and **12** best approximate the experimental IR spectrum (Fig. 7). Taking into account the best agreement found between the calculated UV-Vis spectra of the double hydroxo-bridging and monooxo-bridging structures **9** and **12** with the reflectance spectrum, these two structures can be considered the most probable building blocks that determine the photophysical and vibrational properties of the Zr–AcAc gel.

Conclusions

DFT modeling at the B3LYP/6-31++G(d) level of a series of Zr(IV)–AcAc monomeric and dimeric structural models, and subsequent simulations of their UV-Vis and IR spectra, predicted the most probable building blocks of the Zr(IV)–AcAc sol-gel material. The AcAc-modified Zr(IV) butoxide precursors and AcAc-modified zirconia species formed during the sol-gel process were discussed in accordance with the preparation scheme: exchange, hydrolysis, condensation, and dehydroxylation reactions. It was established that the monomeric Zr(IV)–AcAc unit is the main source of the photophysical properties of the larger Zr chains or rings in the zirconia sol-gel material. Based on the best congruence between the simulated UV-Vis and IR spectra and the corresponding experimental spectra of the Zr–AcAc sol-gel, the dimeric double hydroxo-bridged species $\text{Zr}_2(\text{AcAc})_2(\text{OH})_4(\text{OH})_{2\text{br}}$ (**9**) and the dimeric monooxo bridged species $\text{Zr}_2(\text{AcAc})_2(\text{OH})_4\text{O}_{\text{br}}\cdot 2\text{H}_2\text{O}$ (**12**) were predicted to be the most likely building blocks for the Zr–AcAc gel. In both structures, the two AcAc ligands are coordinated to one Zr atom. The intense absorption band observed at 288 nm was assigned to the intraligand $\pi(\text{AcAc})\rightarrow\pi^*(\text{AcAc})$ transition, whereas the band at 316 nm was attributed to the $\pi(\text{AcAc})\rightarrow\pi^*(\text{AcAc})/d(\text{Zr})$ transition (partial L–M charge transfer character). The calculated IR spectra and assignment of the vibrational frequencies suggested the presence of hydrogen-bonded water molecules, the absence of any butoxide group, and bidentate binding of the AcAc ligands to the Zr atom in the

Zr(IV)–AcAc material. It was shown that the most probable building blocks **9** and **12** determine the photophysical and vibrational properties of the Zr(IV)–AcAc gel.

Acknowledgments The authors thank the National Science Fund of Bulgaria (NSFB) under grants DO-02-233/2008 and DCVP-02/2/2009. S.G. and N.D. were supported by grant TK 02-26/2009 from the NSFB. All computations were performed on the MADARA cluster of the Bulgarian Academy of Sciences.

References

- Hoffmann S, Klee M, Waser R (1995) *Integr Ferroelectr* 10:155–164
- Klee M, Mackens U, Hermann W, Bathelt E (1995) *Integr Ferroelectr* 11:247–258
- Reisfeld R, Zelner M, Patra A (2000) *J Alloys Compd* 300:147–151
- Kuratani K, Mizuhata M, Kajinami A, Deki S (2006) *J Alloys Compd* 408:711–716
- Quan ZW, Wang LS, Lin J (2005) *Mater Res Bull* 40:810–820
- Liu HQ, Wang LL, Chen SG, Zou BS (2008) *J Alloys Compd* 448:336–339
- Petkova N, Dlugocz S, Gutzov S (2011) *J Non-Cryst Solids* 357:1547–1551
- Li Q, Zhong XK, Hu JY, Kang W (2008) *Prog Org Coat* 63:222–227
- Loukova GV, Huhn W, Vasiliev VP, Smirnov VA (2007) *J Phys Chem A* 111:4117–4121
- Kanazhevskii VV, Shmachkova VP, Kotsarenko NS, Kolomiichuk VN, Kochubei DI (2006) *J Struct Chem* 47:453–457
- Devia DH, Sykes AG (1981) *Inorg Chem* 20:910–913
- Bauer M, Gastl C, Koppl C, Kickelbick G, Bertagnolli H (2006) *Monatsh Chem* 137:567–581
- Bauer M, Muller S, Kickelbick G, Bertagnolli H (2007) *New J Chem* 31:1950–1959
- Spijksma GI, Seisenbaeva GA, Fischer A, Bouwmeester HJM, Blank DHA, Kessler VG (2009) *J Sol-Gel Sci Technol* 51:10–22
- Bradley DC, Mehrotra RC, Gaur DP (1978) *Metal alkoxides*. Academic, New York
- Muha GM, Vaughan PA (1960) *J Chem Phys* 33:194–199
- Gutzov S, Borger A, Becker KD (2007) *Phys Chem Chem Phys* 9:491–496
- Schmidt W (2000) *Optische spektroskopie*. Wiley-VCH, Weinheim
- Lee CT, Yang WT, Parr RG (1988) *Phys Rev B* 37:785–789
- Becke AD (1993) *J Chem Phys* 98:5648–5652
- Frisch MJ, Trucks GW, Schlegel HB, Scuseria GE, Robb MA, Cheeseman JR, Scalmani G, Barone V, Mennucci B, Petersson GA, Nakatsuji H, Caricato M, Li X, Hratchian HP, Izmaylov AF, Bloino J, Zheng G, Sonnenberg JL, Hada M, Ehara M, Toyota K, Fukuda R, Hasegawa J, Ishida M, Nakajima T, Honda Y, Kitao O, Nakai H, Vreven T, Montgomery JJA, Peralta JE, Ogliaro F, Bearpark M, Heyd JJ, Brothers E, Kudin KN, Staroverov VN, Kobayashi R, Normand J, Raghavachari K, Rendell A, Burant JC, Iyengar SS, Tomasi J, Cossi M, Rega N, Millam NJ, Klene M, Knox JE, Cross JB, Bakken V, Adamo C, Jaramillo J, Gomperts R, Stratmann EE, Yazyev O, Austin AJ, Cammi R, Pomelli C, Ochterski JW, Martin RL, Morokuma K, Zakrzewski VK, Voth GA, Salvador P, Dannenberg JJ, Dapprich S, Daniels AD, Farkas Ö, Foresman JB, Ortiz JV, Cioslowski J, Fox DJ (2009) *Gaussian 09*, revision A.02. Gaussian Inc., Wallingford
- Andrae D, Haussermann U, Dolg M, Stoll H, Preuss H (1990) *Theor Chim Acta* 77:123–141
- Zhurko GA, Zhurko DA (2011) ChemCraft software package. <http://www.chemcraftprog.com>
- Cances E, Mennucci B, Tomasi J (1997) *J Chem Phys* 107:3032–3041
- Cossi M, Barone V, Mennucci B, Tomasi J (1998) *Chem Phys Lett* 286:253–260
- Mennucci B, Tomasi J (1997) *J Chem Phys* 106:5151–5158
- Schirmer J (1982) *Phys Rev A* 26:2395–2416
- Trofimov AB, Schirmer J (1995) *J Phys B* 28:2299–2324
- Hattig C, Weigend F (2000) *J Chem Phys* 113:5154–5161
- Weigend F, Ahlrichs R (2005) *Phys Chem Chem Phys* 7:3297–3305
- Hattig C (2003) *J Chem Phys* 118:7751–7761
- Kohn A, Hattig C (2003) *J Chem Phys* 119:5021–5036
- Ahlrichs R, Bar M, Haser M, Horn H, Kolmel C (1989) *Chem Phys Lett* 162:165–169
- Reed AE, Curtiss LA, Weinhold F (1988) *Chem Rev* 88:899–926
- Cueto LF, Sanchez E, Torres-Martinez LM, Hirata GA (2005) *Mater Charact* 55:263–271
- Jones AC (2002) *J Mater Chem* 12:2576–2590
- Kessler VG, Seisenbaeva GA, Werndrup P, Parola S, Spijksma GI (2005) *Mater Sci Poland* 23:69–78
- Hoebbel D, Reinert T, Schmidt H, Arpac E (1997) *J Sol-Gel Sci Technol* 10:115–126
- Morris S, Almond MJ, Cardin CJ, Drew MGB, Rice DA, Zubavichus Y (1998) *Polyhedron* 17:2301–2307
- Greenwood NN, Earnshaw A (1984) *Chemistry of the elements*. Pergamon, Oxford
- Bradley DC, Thornton P (1979) *Zirconium and hafnium*. Pergamon, Oxford
- Radtke A, Piszczek P, Muziol T, Wojtczak A, Grodzicki A (2010) *Struct Chem* 21:367–375
- Ekberg C, Kallvenius G, Albinsson Y, Brown PL (2004) *J Sol Chem* 33:47–79
- Linstrom PJ (2011) NIST Chemistry WebBook. <http://webbook.nist.gov/chemistry>
- Nakamoto K (1978) *Infrared and Raman spectra of inorganic and coordination compounds*. Wiley, New York
- Tarte P (1958) *Spectrochim Acta* 13:107–119
- Piszczek P, Grodzicki A, Richert M, Radtke A (2005) *Mater Sci Poland* 23:663–670